Cancer Research

VEGF-PET Imaging Is a Noninvasive Biomarker Showing Differential Changes in the Tumor during Sunitinib Treatment

Wouter B. Nagengast[1], Marjolijn N. Lub-de Hooge[2,3], Sjoukje F. Oosting[1], Wilfred F.A. den Dunnen[4], Frank-Jan Warnders[1], Adrienne H. Brouwers[3], Johan R. de Jong[3], Patricia M. Price[5], Harry Hollema[4], Geke A.P. Hospers[1], Philip H. Elsinga[3], Jan Willem Hesselink[6], Jourik A. Gietema[1], and Elisabeth G.E. de Vries[1]

Abstract

Non-invasive imaging of angiogenesis could ease the optimization of antiangiogenesis treatments for cancer. In this study, we evaluated the role of VEGF-PET as a biomarker of dynamic angiogenic changes in tumors following treatment with the kinase inhibitor sunitinib. The effects of sunitinib treatment and withdrawal on the tumor was investigated using the new VEGF-PET tracer ^{89}Zr-ranibizumab as well as ^{18}F-FDG PET, and ^{15}O-water PET in mouse xenograft models of human cancer. The obtained imaging results were compared with tumor growth, VEGF plasma levels and immunohistologic analyzes. In contrast to ^{18}F-FDG and ^{15}O-water PET, VEGF-PET demonstrated dynamic changes during sunitinib treatment within the tumor with a strong decline in signal in the tumor center and only minimal reduction in tumor rim, with a pronounced rebound after sunitinib discontinuation. VEGF-PET results corresponded with tumor growth and immunohistochemical vascular- and tumor- markers. Our findings highlight the strengths of VEGF-PET imaging to allow serial analysis of angiogenic changes in different areas within a tumor. *Cancer Res; 71(1); 143–53. ©2010 AACR.*

Introduction

Angiogenesis, the formation of new blood vessels, is one of the hallmarks of carcinogenesis. VEGF and its corresponding receptors (VEGFR) on endothelial cells are important players in the regulation of angiogenesis, providing targets for anti-angiogenic agents (1). When used either as single agents or combined with chemotherapy, antiangiogenic drugs have improved disease outcome in several tumor types. However, this benefit is modest and often of limited duration. Further, unexplained paradoxical effects have been observed. For example, the VEGFR tyrosine kinase inhibitor (TKI) sunitinib is used for the clinical treatment of metastatic renal cell cancers and gastrointestinal stromal tumors as it blocks angiogenesis in primary tumors (2), but its use may also lead to increased invasiveness at the tumor boundary and promotion of metastases (3, 4). This complex and dynamic interaction between tumor cells and their microenvironment may be an important reason why previous investigation of potential biomarkers has failed to predict response to antiangiogenic therapy. The search for biomarkers has been especially directed towards circulating markers and visualizing anatomic tumor changes during antiangiogenic treatment (4). The biological responses that occur in response to antiangiogenic treatment are presumably dynamic over time and likely to be heterogeneous within the tumor. Therefore molecular imaging, enabling visualization of biological processes, might provide a better insight into how tumors respond to anti-angiogenic treatment with agents such as sunitinib.

Well known techniques for molecular imaging include measurement of tissue glucose uptake with ^{18}F-FDG positron emission tomography (PET) to assess metabolism and measurement of tissue perfusion with ^{15}O-water PET. A new option is direct imaging the molecules involved in the promotion or inhibition of VEGF signaling using PET analysis, which may be achieved following molecular radiolabeling. Therapeutic inhibitors of the VEGF pathway, such as the monoclonal antibody bevacizumab and the antibody derivative ranibizumab, which bind and block VEGF-A, have proven clinical antiangiogenic effectiveness and are attractive for this purpose (5, 6).

Previously, we developed ^{89}zirconium-labeled bevacizumab (^{89}Zr-bevacizumab) as a biomarker for the PET analysis of VEGF levels, with the aim of providing insight into the available target for VEGF-dependent antiangiogenic therapy

Authors' Affiliations: Departments of [1]Medical Oncology, [2]Hospital and Clinical Pharmacy, [3]Nuclear Medicine and Molecular Imaging, and [4]Pathology, University of Groningen and University Medical Center Groningen, Groningen, the Netherlands; [5]Academic Department of Radiation Oncology, The Christie Hospital, Manchester, United Kingdom; and [6]Department of Surgery, University of Groningen and University Medical Center Groningen, Groningen, the Netherlands

Note: Supplementary data for this article are available at Cancer Research Online (http://cancerres.aacrjournals.org/).

Corresponding Author: Elisabeth G. de Vries, Department of Medical Oncology, University Medical Center Groningen, Groningen Hanzeplein 1, Postbus 30.001, 9700 RB Groningen, the Netherlands. Phone: 31-50-361-2821/1847; Fax: 31-50-361-4862. E-mail: E.G.E.de.Vries@int.umcg.nl

doi: 10.1158/0008-5472.CAN-10-1088

and thus assist in tumor response prediction (6). This approach proved promising, as tumor uptake of ^{89}Zr-bevacizumab mediated by VEGF-A binding significantly higher than control antibody was demonstrated, providing a potential new tracer for noninvasive imaging of VEGF signaling in the microenvironment of the tumor. Further, the ^{89}Zr label, with its half life of 78 hours, proved valuable for antibody imaging allowing high-resolution PET over at least 24 hours. However, maximum uptake did not occur until 4 to 7 days post injection (pi ; ref. 6), likely due to the 21 days serum half-life of bevacizumab (7). To gain more dynamic insight into tumor response during antiangiogenic treatment, we have since developed the PET tracer ^{89}Zr-ranibizumab for potential use as noninvasive biomarker of VEGF signaling. Ranibizumab, a monoclonal antibody fragment (Fab) derivative of bevacizumab, is used to treat macular degeneration (8). It has a higher affinity for all soluble and matrix bound human VEGF-A isoforms than bevacizumab (7). In addition, it allows fast and sequential follow up PET scans, as its serum half-life is only 2 to 6 hours.

In this study, we investigated the biological effects of sunitinib treatment and subsequent withdrawal in human xenograft tumor models, using tumor growth assays, immunohistochemistry, and PET analyses (^{18}F-FDG, ^{15}O-water, and ^{89}Zr-ranibizumab). A secondary aim was to determine the utility of ^{89}Zr-ranibizumab-PET analysis as a biomarker for antiangiogenic treatment.

Methods

Cell lines and *in vitro* experiments

The human ovarian tumor cell lines A2780 (provided by Dr TC Hamilton, Fox Chase Cancer Center). The human ovarian cancer cell line SKOV-3 and the human colon cancer cell line Colo205 were obtained from the ATCC. Cell lines were quarantined until screening for microbial contamination and mycoplasm were performed and proven to be negative. Meanwhile, a reproducible supply of cells was established by cryopreservation. All experiments were performed within a predefined number of passages. Key features of the cell lines were routinely checked. Growth and morphology of both cell lines was observed and noted to be consistent with prior descriptions of the lines; no further genetic characterization was performed. A2780 and Colo205 were cultured in RPMI-1640 (Invitrogen) with 10% heat-inactivated fetal calf serum (FCS; Bodinco BV) and 2 mmol/L of L-glutamine (Invitrogen) at 37°C in a humidified atmosphere containing 5% CO_2, SKOV-3 in Dulbecco's modified Eagles medium with 4.5 g/mL of glucose and 10% FCS. Cells were subcultured 3 times per week.

For *in vitro* experiments sunitinib (LC Laboratories) was dissolved in dimethyl sulfoxide (DMSO) at 40 mg/mL and stored at −80 °C. The MTT assay was used to determine cytotoxicity of sunitinib in A2780 and Colo205 cells (9). Cells were seeded (A2780 3,750 cells per well, Colo205 3,000 cells per well) in a 96-well plate in quadruplicate for each sunitinib concentration (0–20,000 nmol/L) and cultured for 4 days. No cytotoxicity occurred at sunitinib levels up to 5,000 nmol/L, which is a relevant plasma level in mice (Supplement 1).

^{18}F-FDG and ^{15}O-water synthesis

^{18}F-FDG was produced using the coincidence ^{18}F-FDG synthesis module (10). Carrier-added [^{15}O]O_2 was produced by irradiation of a mixture of nitrogen and 1% oxygen gas with 7 MeV deuterons from a Scanditronix MC-17 cyclotron. [^{15}O]O_2 was reacted with hydrogen gas at 400°C to generate ^{15}O-water. The ^{15}O-water was trapped in a sterivial with 2.5 mL of 0.9% NaCl and sterilized by filtration (22-μm Millex GP filter).

Conjugation and ^{89}Zr-labeling of ranibizumab and control Fab-IgG

Conjugation and labeling of ranibizumab (Lucentis, Novartis Pharma) and Fab-IgG were executed as described for U36 (6, 11). The chelate desferrioxamine B (Df; Novartis Pharma) was succinylated (*N*-sucDf), and coupled to lysine residues of ranibizumab by means of a tetrafluorophenol-*N*-sucDf ester. Conjugation was performed at room temperature for 30 minutes at pH 9.5 to 9.7. Hereafter, the mixture was adjusted to pH 4.2 to 4.4 (0.1 mol/L of H_2SO_4) and 50 μL of 25 mg/mL of ethylenediaminetetraacetic acid (EDTA; Calbiochem) was added to remove Fe(III). The resultant solution was then purified by ultrafiltration, diluted in water for injection (5 mg/mL) and stored at −20°C. Labeling was performed with ^{89}Zr produced by Cyclotron BV. ^{89}Zr-oxalate was adjusted to pH 3.9 to 4.2 and mixed for 3 minutes, then adjusted to pH 6.7 to 6.9 using HEPES buffer. N-sucDf-ranibizumab was added and incubated for 45 minutes at 20°C. ^{89}Zr-ranibizumab labeling (specific activity [SA] 1,500 MBq/mg) resulted in yields of more than 95%. 24 hours storage in 37°C serum displayed no measurable decrease in protein-bound radioactivity and revealed adequate VEGF-A binding, comparable to unlabeled ranibizumab using a VEGF-coated enzyme-linked immunosorbent assay as described previously for bevacizumab (Supplement 2; 6). Control ^{89}Zr-Fab-IgG is a humanized Fab-fragment comparable in size to ranibizumab. It was similarly prepared and showed no binding affinity toward VEGF-A.

Animal experiments

Animal experiments were performed with isofluran inhalation anesthesia (induction 3%, maintenance 1.5%). Tumor cells for xenografting were harvested by trypsinization and resuspended in culture medium and Matrigel (BD Bioscience). *In vivo* imaging and *ex vivo* biodistribution experiments were conducted using male nude HSD athymic mice (Harlan). 6 to 8 weeks old mice were injected subcutaneously with 1.0×10^5 SKOV3, 5×10^6 A2780, 5×10^6 A2780^{luc+}, or 5×10^6 Colo205 cells mixed with 0.1 mL Matrigel™. *In vivo* studies were commenced when resulting tumors measured 6 to 8 mm in diameter. All animal experiments were approved by the animal experiments committee of the University of Groningen.

MicroPET imaging and *ex vivo* biodistribution

All tracers were injected intravenously into the penile vein. ^{18}F-FDG (5.0 ± 1.0 Mbq) microPET images (Focus 220 rodent scanner (CTI Siemens)) were obtained 1 hour pi. Animals were

fasted for 12 hours before ^{18}F-FDG administration. Ten minutes dynamic PET imaging was taken after ^{15}O-water (78 ± 8.9 Mbq) administration followed by microCT imaging using a MicroCAT II (CTI Siemens) for anatomic localization. ^{89}Zr-ranibizumab (3.5 ± 1.5 Mbq) images were taken 0, 3, 6, and 24 hours pi. Static images of 30 minutes acquisition time were obtained each time.

Following image reconstruction, quantification was performed with AMIDE Medical Image Data Examiner software (version 0.9.1, Stanford University; ref. 12). To quantify radioactivity within the tumor, 3D volumes of interest (VOIs) were drawn. ^{18}F-FDG is presented as standardized uptake value (SUV), using mean tumor uptake per cm^3 divided by mean body uptake. ^{15}O-water is presented as percentage uptake per cm^3 relative to tumor uptake in the first frame (30 seconds) of the scan. For ^{89}Zr-ranibizumab, the total injected dose was calculated by decay correction of total activity present at 0 hour after injection in the animal. The data were quantified as percentage injected dose per gram (%ID/g), assuming a tissue density of 1. Data are presented as percentage uptake compared with baseline and corrected for tumor volume. Following sacrifice, organs and tissues were excised, rinsed for residual blood, and weighed. Samples and primed standards were counted for radioactivity in a well-type LKB-1282-Compu-gamma system (LKB Wallac) and corrected for physical decay. Harvested tumors were divided, immediately frozen at −80°C, and paraffin embedded for further analysis.

Dose finding study and pharmacokinetics of ^{89}Zr-ranibizumab

On the basis of available ^{89}Zr-bevacizumab data for comparison (5), we firstly used the SKOV-3 xenograft model to evaluate ^{89}Zr-ranibizumab characteristics. In 4 groups of animals, 4 protein doses [3, 8, and 40 μg (all $n = 4$) and 350 μg ($n = 1$)] ranibizumab labeled with a fixed amount (MBq) of ^{89}Zr were administered and biodistribution was determined 24-hours pi. Subsequently, 4 groups ($n = 4$) of mice were injected with 5 μg of ^{89}Zr-ranibizumab and 1, 3, 6, and 24 hours thereafter a group was sacrificed and *ex vivo* biodistribution performed. One group of mice ($n = 4$) was injected with 5 μg of ^{89}Zr-Fab-IgG. *Ex vivo* biodistribution followed 24-hours pi.

Sunitinib treatment in A2780 and Colo205 models

Sunitinib malate was dissolved in DMSO at 75 mg/mL. Before administration, sunitinib was diluted in phosphate-buffered saline (PBS; 140 of mmol/L of NaCl, 9 mmol/L of Na_2HPO_4, 1.3 mmol/L of NaH_2PO_4; pH = 7.4) and administrated intraperitoneally (ip) once daily at 60 mg/kg (6.5 mL/kg) or placebo (vehicle). Sixty milligram per kilogram of sunitinib daily previously demonstrated antitumor efficacy in xenograft-bearing mice and changes in tumor-derived human VEGF plasma levels with minimal toxicity (13). Four different treatment schedules with once daily ip treatment were used. ^{18}F-FDG imaging was performed in A2780-bearing animals at baseline ($n = 4$), day 7 ($n = 4$) of sunitinib treatment and following a drug-free week ($n = 5$). Serial ^{15}O-water PET was carried out in A2780-bearing animals ($n = 5$) at baseline and following 7 days of sunitinib. Serial ^{89}Zr-ranibizumab imaging (5 ± 1 μg) was performed in A2780-bearing mice treated with sunitinib for 1 week followed by a drug-free week ($n = 4$), sunitinib ip for 2 weeks ($n = 4$), sunitinib for 1 week ($n = 4$), or placebo treatment ($n = 4$) and Colo205 tumor bearing mice with sunitinib for 1 week followed by a drug-free week ($n = 5$) at baseline, day 7 and day 14. To assess relative attribution of non-VEGF driven uptake, serial ^{89}Zr-Fab-IgG imaging was performed in A2780-bearing animals ($n = 5$) at baseline, day 7 of sunitinib and following a drug-free week. Tumor volumes were assessed by external calibration along the longest axis (x-axis) and the axis perpendicular to the longest axis (y-axis). Tumor volume was calculated by the formula: $(x \times y^2)/2$.

Plasma human VEGF analysis and tumor immunohistochemistry

Plasma VEGF levels of sacrificed A2780-bearing mice were determined with the human VEGF ELISA kit (R&D Systems). Paraffin-embedded tumors (n = 4 per treatment group) were stained with hematoxylin and eosin and antibodies against von Willebrand factor (vWf), Ki67 anti-human and anti-mouse (Dako), VEGFR2 (Cell Signaling), GLUT-1 (Chemicon), HIF1α (BD Biosciences), and human VEGF-A (sc-152, Santa Cruz). The mean vascular density (MVD) and VEGFR2 were scored in 3-defined hot spot areas that contained the maximum number of microvessels, as previously described (6). To assess changes in tumor vessel diameter, the shortest diameter of the largest vessels (≥5 per slide) were measured using computerized Aperio Image Software (Aperio Technologies Inc). Blood vessel proliferation was determined by calculating the percentage blood vessels with Ki67-positive endothelial cells. The tumor proliferation index was calculated by percentage of Ki67-positive cells in at least 4 high-power fields (200×). MVD, tumor vessel diameter, VEGFR2, blood vessel proliferation, and tumor proliferation were obtained for tumor rim (area < 500 μm of tumor margin) and center (area > 500 μm of tumor margin). GLUT-1 and HIF1α staining was scored manually as percentage positive of total tumor tissue per slide.

Statistical analysis

Data are presented as means ± SEM. Statistical analysis was performed using the Mann–Whitney U test for unpaired data and the Wilcoxon Matched Pairs test for paired data (SPSS, version 14). Tumor growth curves (trends) were analyzed using linear regression analyses. All tests were 2 sided and the significance level was taken as 0.05 or less.

Results

Sunitinib reduces tumor growth, but rapid regrowth occurs after discontinuation

Sunitinib treatment was evaluated in the A2780 and Colo205 model, which were chosen for their angiogenic profile and constant growth rate (2, 14). In A2780-bearing mice, tumor growth diminished after 7 days of daily sunitinib treatment. Tumors in treated animals increased 123.7% ± 16.0% from baseline, compared with 182.0% ± 18.1% in nontreated animals

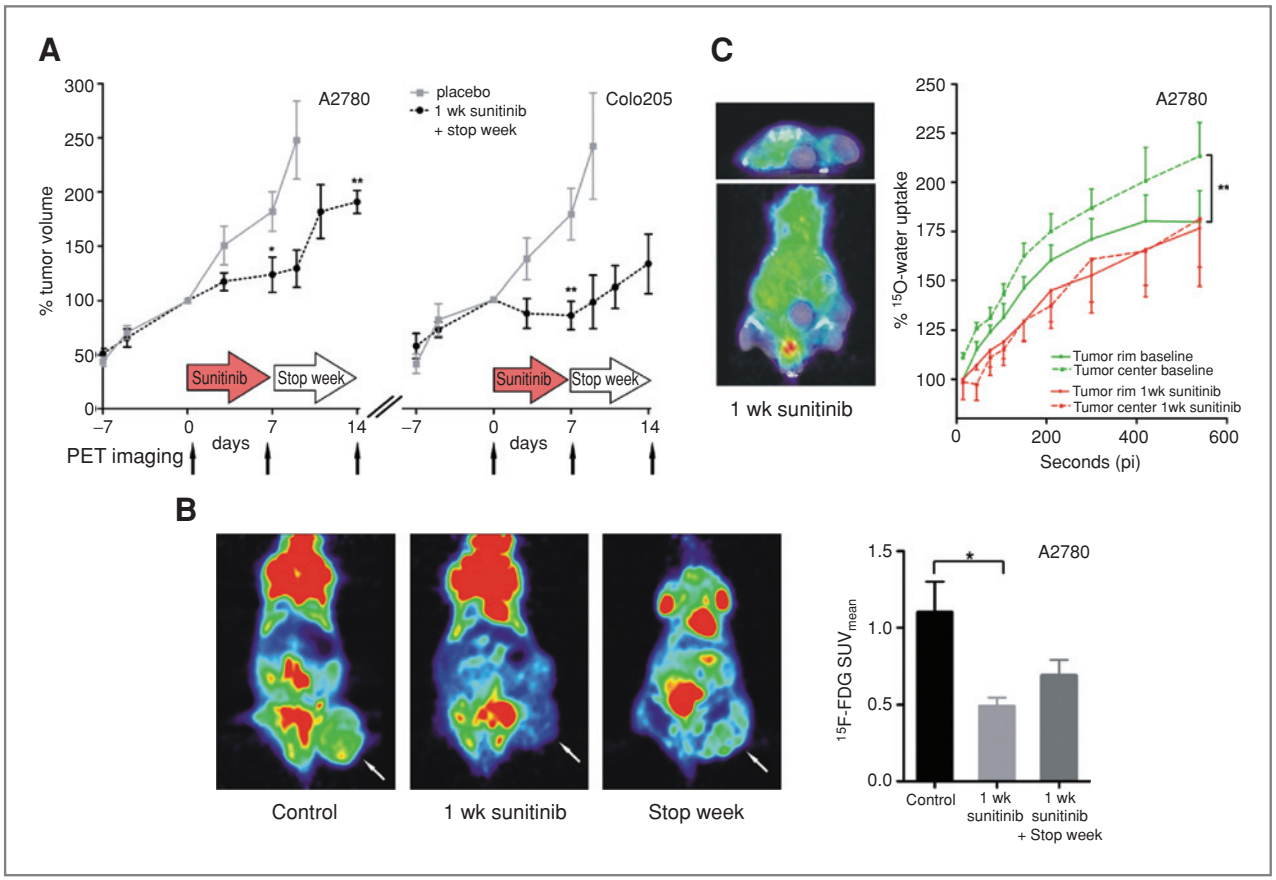

Figure 1. A, tumor volumes of A2780 and Colo205 treated tumors. Tumor volumes were normalized to the start of sunitinib treatment. B, representative coronal ^{18}F-FDG microPET images of nontreated A2780-bearing mice, following 1 week of sunitinib treatment and after 1 week of sunitinib treatment plus a stop week (nonpaired animals are presented) and ^{18}F-FDG uptake quantification in control A2780-treated tumors, after 1 week of sunitinib treatment and after 1 week of sunitinib treatment plus a stop week. C, representative fused transversal and coronal ^{15}O-water PET/CT image after 1 week sunitinib in A2780-bearing mice and normalized ^{15}O-water PET quantification at baseline and following 1 week of sunitinib. *, $P < 0.05$; **, $P < 0.01$. *Data presented as SEM.*

(Fig. 1A). Thereafter sunitinib was withdrawn for 7 days and tumor growth accelerated to 190% ± 10.8% on day 14. Tumor growth tended to be slower when sunitinib was continued, resulting in a tumor volume of 140.0% ± 16.1% at day 14 compared with day 0 ($P = 0.067$). In the Colo205 model, sunitinib induced significant tumor growth stabilization at day 7 after daily sunitinib treatment. When sunitinib was withdrawn, tumors showed regrowth, from an average volume of 86.6% ± 12.9% on day 7 to 132.9% ± 26.8% on day 14 ($P = 0.096$), with a significant tumor growth curve from zero ($P = 0.0006$).

Molecular imaging with ^{18}F-FDG PET and ^{15}O-water PET

At baseline, ^{18}F-FDG PET showed a homogeneous tumor uptake in A2780 tumor-bearing animals (Fig. 1B). Seven days of sunitinib treatment resulted in a 55% homogeneous decrease in ^{18}F-FDG uptake compared with nontreated animals. When sunitinib treatment was stopped, ^{18}F-FDG uptake on day 14 was slightly higher than on day 7.

^{15}O-water PET in A2780 tumors showed a 3- to 8-fold lower uptake at baseline than well perfused organs such as heart and kidneys, resulting in suboptimal tumor visualization (Fig. 1C). Further, ^{15}O-water PET tumor uptake at baseline was 15.8% higher in the center compared with the tumor rim. By day 7 of sunitinib treatment, tumor uptake tended to decrease in the center compared with baseline (−16.8% ± 7.7%), though not significantly ($P = 0.11$) and no difference between tumor rim and center was observed.

Molecular tumor imaging using ^{89}Zr-ranibizumab PET

^{89}Zr-ranibizumab was first evaluated in the SKOV-3 model. Within 3 hours pi of ^{89}Zr-ranibizumab clear tumor visualization was seen (Fig. 2A), with a plateau at 24 hours (Fig. 2B). At 24 hours, ^{89}Zr-ranibizumab tumor uptake was 2.54-fold higher than ^{89}Zr-Fab-IgG (3.96% ± 1.00% ID/g vs. 1.56% ± 0.38% ID/g, $P = 0.034$), signifying VEGF-A specificity of ^{89}Zr-ranibizumab uptake. Increasing doses of unlabeled ranibizumab blocked tumor uptake of ^{89}Zr-ranibizumab to the uptake level of ^{89}Zr-Fab-IgG (Fig. 2B). Furthermore, organ biodistribution revealed rapid blood clearance of ^{89}Zr-ranibizumab from 8.44% ± 2.19% ID/g 1 hour pi to 0.38% ± 0.38% ID/g 24 hours

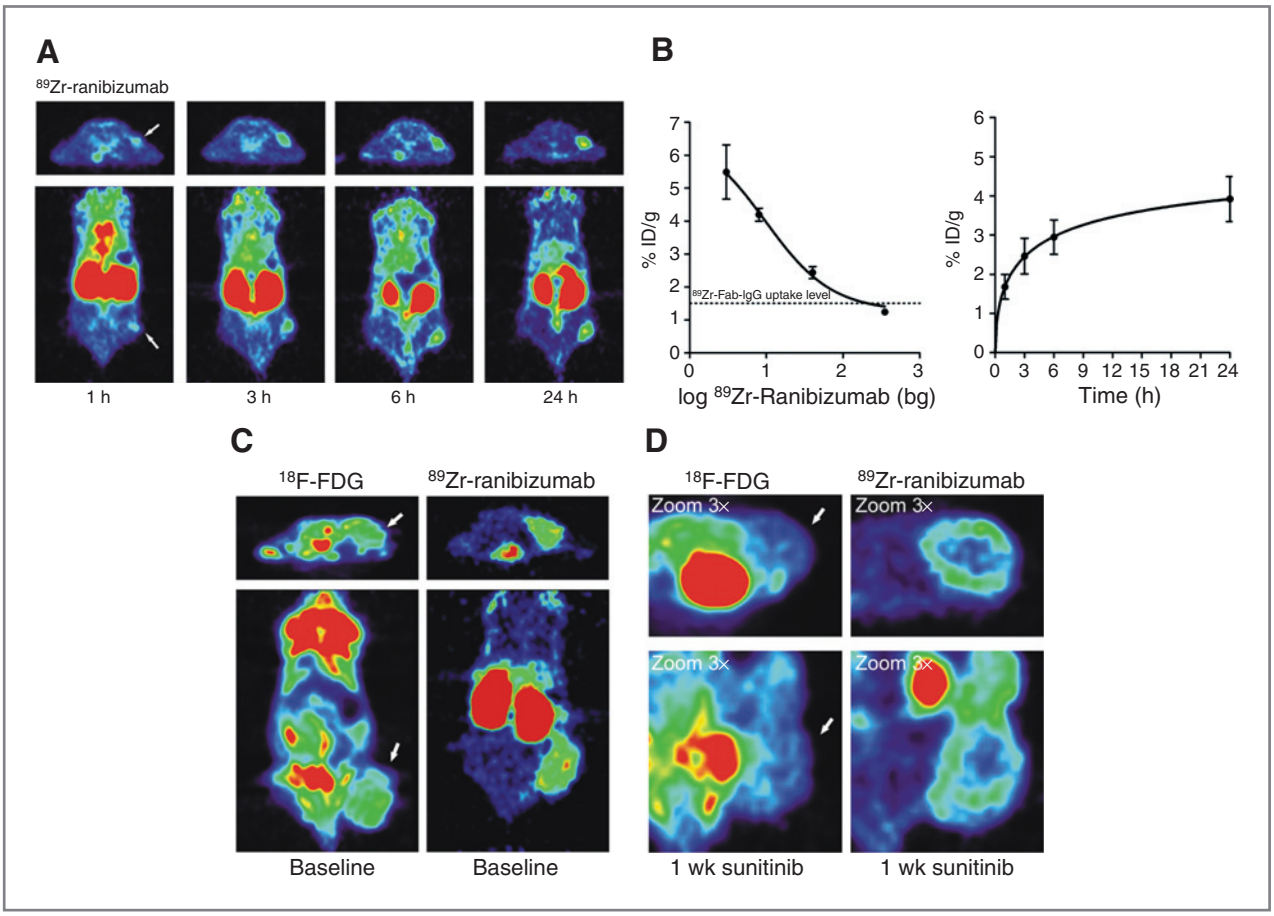

Figure 2. A, representative transversal and coronal microPET images of ^{89}Zr-ranibizumab 1, 3, 6, and 24 hours pi in SKOV-3 xenograft. B, relative tumor uptake versus injected protein dose of ^{89}Zr-ranibizumab in SKOV-3 xenograft model (dotted line shows ^{89}Zr-Fab-IgG tumor uptake) and time distribution curve of ^{89}Zr-ranibizumab uptake in SKOV-3 xenograft model. C, transversal and coronal microPET image of ^{18}F-FDG (1 hour pi) and ^{89}Zr-ranibizumab (24 hours pi) at baseline in A2780 xenograft (paired sample) with clear tumor visualization. D, following 1 week sunitinib ^{18}F-FDG uptake in the tumor decreases homogeneously, whereas ^{89}Zr-ranibizumab uptake is still high in the tumor rim (paired sample). Tumor indicated by arrow.

pi resulting in tumor/blood ratios higher than 10 (Supplement 3).

Sunitinib decreases ^{89}Zr-ranibizumab tumor uptake, especially in the tumor center, with a marked rebound after discontinuation

In the next experiments ^{89}Zr-ranibizumab quantification was performed 24 hours pi unless otherwise stated. At baseline, ^{89}Zr-ranibizumab uptake was 8.75% lower in the tumor rim than in the center ($P = 0.05$), comparable to findings seen with ^{15}O-water PET. In A2780 placebo-treated mice, ^{89}Zr-ranibizumab (% ID/g) tumor uptake remained constant between baseline and 1 week (Δ 8%, $P = 0.229$). However after 7 days of sunitinib treatment in A2780 and Colo205 xenografts, there was a pronounced reduction in ^{89}Zr-ranibizumab tumor uptake in the tumor center but minimal effect in the tumor rim, whereas ^{18}F-FDG decreased homogeneously (Fig. 2D). In A2780 tumors, ^{89}Zr-ranibizumab uptake decreased by only 19.5% $\pm$ 5.1% in the rim, whereas a decrease of 45.4% $\pm$ 5.9% was found in the center compared with baseline (Fig. 3B). Control experiments with ^{89}Zr-Fab-IgG, showed only a minimal decrease in uptake at day 7 following sunitinib treatment in A2780 tumors, indicating minimal changes in nonspecific uptake of Fab fragments following sunitinib treatment. In contrast, decreased ^{89}Zr-ranibizumab uptake was 3.2-fold greater than control ^{89}Zr-Fab-IgG experiments (Fig. 3D). Interestingly, in A2780 tumors treated for 14 days, ^{89}Zr-ranibizumab uptake in the rim increased 46% at day 14 compared with day 7 (Fig. 3D), whereas in the center the uptake remained low compared with baseline.

PET scans performed 7 days after stopping sunitinib treatment showed higher ^{89}Zr-ranibizumab tumor uptake in both models, which exceeded baseline values. In A2780, ^{89}Zr-ranibizumab tumor rim uptake increased 69.5% $\pm$ 18.3% versus 7 days sunitinib, and 34.6% $\pm$ 11.4% ($P = 0.056$) versus baseline (Fig. 3B). Likewise, uptake in the tumor center increased and returned to baseline. In Colo205 tumors, ^{89}Zr-ranibizumab uptake in the tumor center exceeded baseline values (31.7% $\pm$ 9.9%; $P = 0.033$) 7 days after discontinuation (Supplement 4 and 5). Control experiments using ^{89}Zr-Fab-IgG showed some enhancement

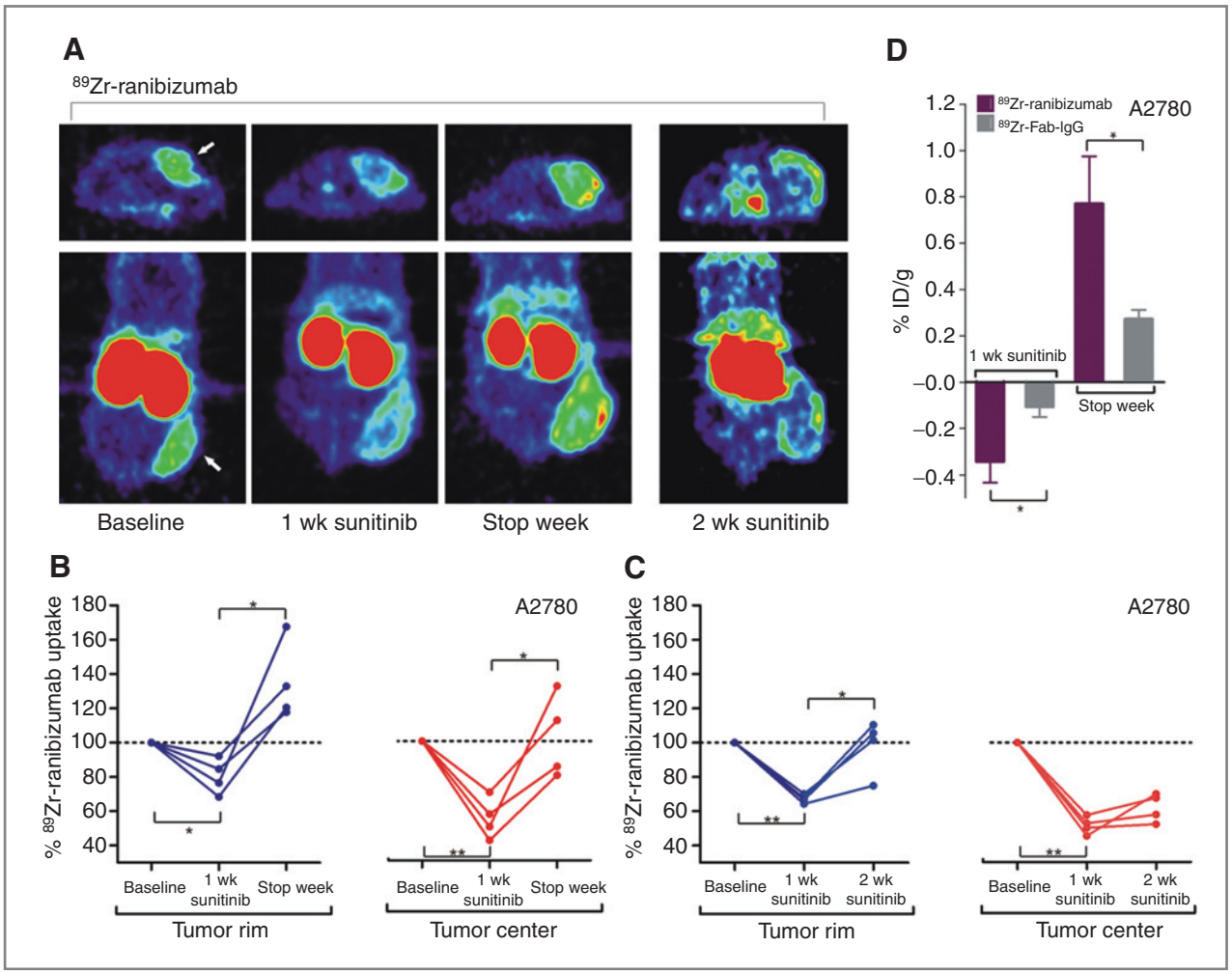

Figure 3. A, transversal and coronal microPET images of ^{89}Zr-ranibizumab at 24 hours pi of the tracer. High tumor to background ratios clearly visualize a more pronounced reduction in the tumor center compared with the tumor rim after 7 day of sunitinib treatment. After 7 days of discontinuation, ^{89}Zr-ranibizumab uptake increases (paired samples). At day 14 of sunitinib treatment, ^{89}Zr-ranibizumab uptake returns to baseline in the tumor rim while remaining low in the tumor center. B, ^{89}Zr-ranibizumab quantification of tumor rim and center of mice treated with sunitinib for 1 week at day 7 and following a stop week and after 14 days (C) of sunitinib treatment. Individual tumor uptake values are normalized relative to baseline. D, change in average tumor uptake (both rim and center) of ^{89}Zr-ranibizumab and ^{89}Zr-Fab-IgG after 7 days of sunitinib and after a stop week in A2780 xenograft model. *, $P < 0.05$; **, $P < 0.01$. *Data presented as SEM.*

in passive tumor uptake, but were 2.83-fold lower than with ^{89}Zr-ranibizumab.

Differential tumor response on ^{89}Zr-ranibizumab-PET scan between tumor rim and center corresponds with microscopic changes. Histologic examination also revealed a differential effect of sunitinib on the tumor rim and center. After 7 days of sunitinib treatment, nonaffected blood vessels were mainly present in the tumor rim. Tumor tissue surrounding these vessels retained a high proliferation rate, and low HIF1α and GLUT-1 expression (Fig. 4A). Tumor tissue surrounding affected vessels in the center showed a low tumor proliferation rate, high HIF1α, and GLUT-1 expression. The center contained predominantly vital areas with some areas of necrosis (Supplement 7). Seven days of sunitinib treatment resulted in a reduction in all vascular markers and decreased tumor cell proliferation, which was most pronounced in the tumor center (Supplement 8). Interestingly, at day 14 the tumor blood vessel diameter returned to baseline and increased tumor proliferation rate was observed in the tumor rim, which coincided with increased VEGF-A staining. Interestingly, no changes in vascular markers or tumor and endothelial proliferation were observed in the tumor center compared with day 7.

After a 7 day drug-free period, all vascular makers recovered and tumor vessel diameter even exceeded baseline. In addition, HIF1α and GLUT-1 expression decreased whereas an increased VEGF-A expression and tumor proliferation were observed (Fig. 4 and Fig. 5). Furthermore, large areas of randomly distributed multiple blood-filled regions (pelioses) were present at baseline and after discontinuation in parallel with high endothelial proliferation (Fig. 4D). Together these findings indicate rapid tumor revascularization after stopping sunitinib, which closely matches *in vivo* PET findings.

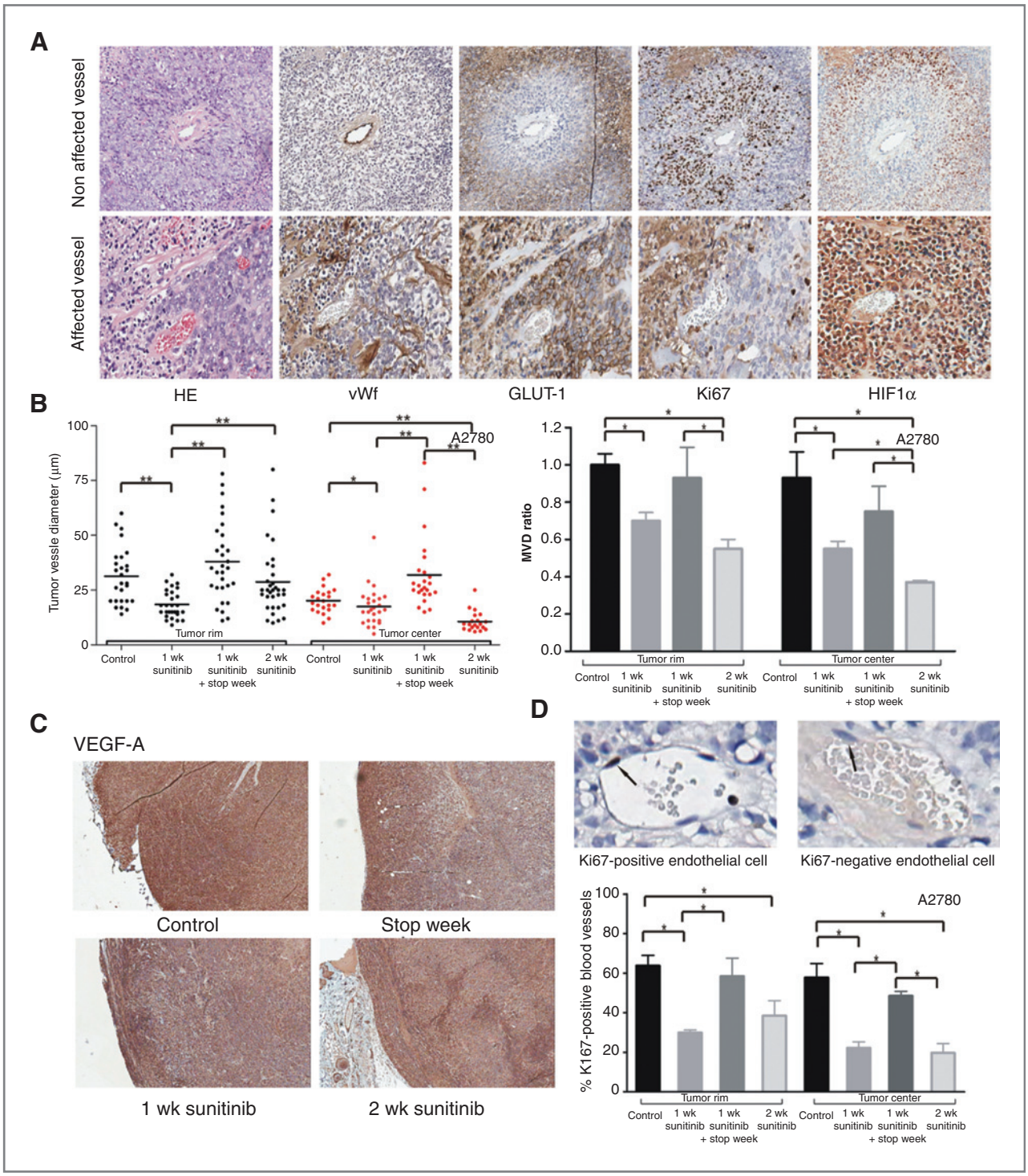

Figure 4. A, representative examples of A2780 illustrating affected and nonaffected tumor vessels following 7 days of sunitinib treatment. Nonaffected vessels demonstrate clear vWf staining with low GLUT-1 expression, high Ki67 staining and low HIF1α expression in the surrounding tumor tissue which is the opposite for affected tumor vessels. B, tumor vessel diameter of tumor rim and center and MVD quantification of the tumor rim and center. C, representative VEGF-A staining. D, percentage of tumor vessels containing Ki67 positive endothelial cells in tumor rim and center. *, $P < 0.05$, **, $P < 0.01$. *Data presented as SEM.*

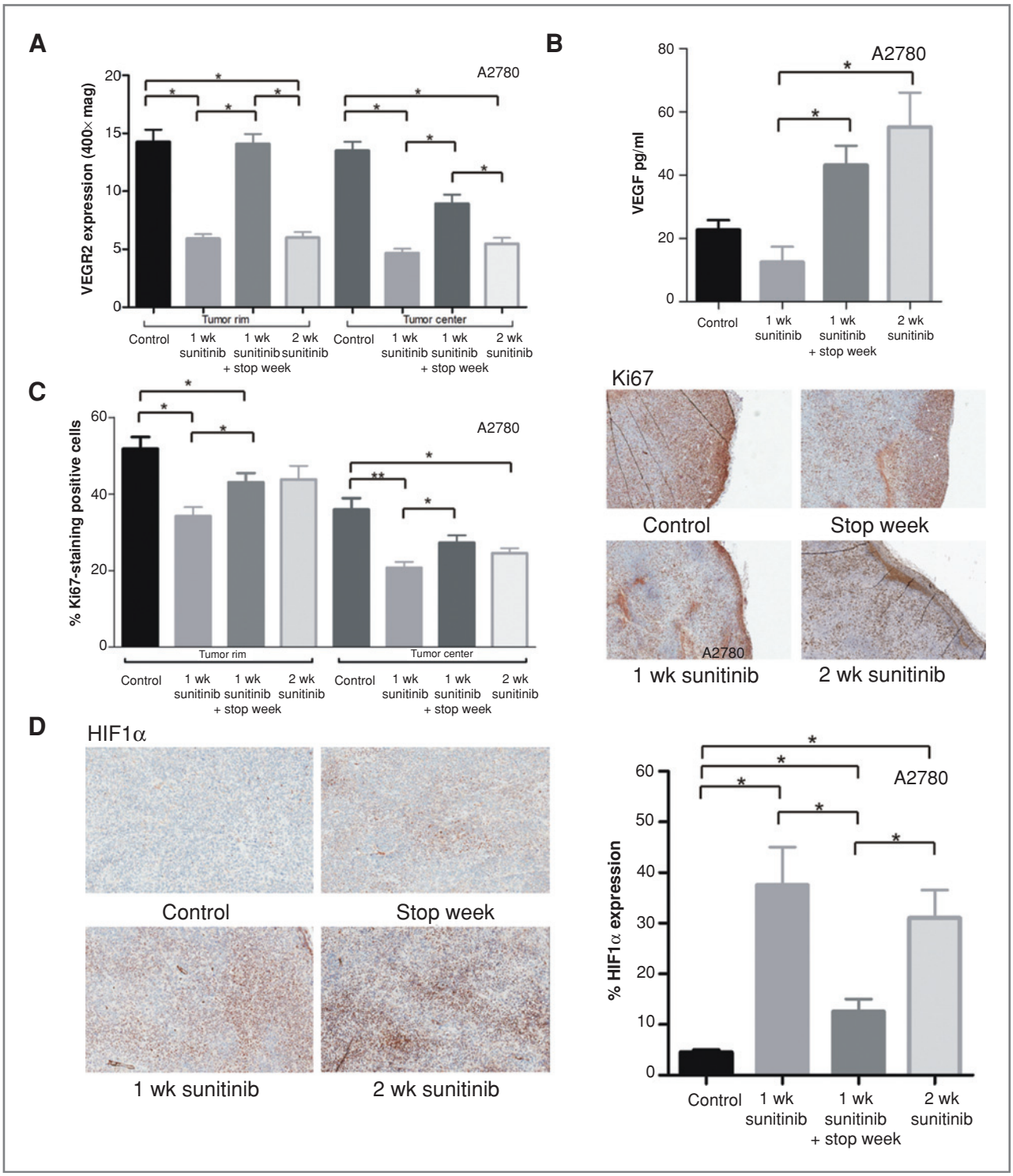

Figure 5. A, VEGFR2 staining in the tumor rim and center. B, human VEGF plasma levels of sacrificed A2780-bearing animals. C, tumor proliferation rate at the tumor rim and center. After 7 days of sunitinib overall tumor proliferation decreases, though it remains high at the rim. D, tumor HIF1α expression is high after 1 and 2 weeks of sunitinib treatment. After the stop week, HIF1α decreases towards baseline. *, $P < 0.05$; **, $P < 0.01$. *Data presented as SEM.*

Changes in tumor derived human plasma VEGF levels

After 7 days of sunitinib treatment, tumor derived human VEGF plasma levels decreased by 60% (Fig. 5B), whereas after 14 days of sunitinib treatment there was a 6.61-fold increase compared with day 7. After the 7 day drug-free period a 4.79-fold increase was observed.

Discussion

This study is the first to investigate the effect of sunitinib treatment and its withdrawal on tumor biology using the molecular imaging techniques ^{89}Zr-ranibizumab-PET, ^{18}F-FDG PET, and ^{15}O-water PET in human xenograft tumor models. ^{89}Zr-ranibizumab-PET corresponded best with findings observed by tumor proliferation and vascularization assays, histology, and immunohistochemistry. Strikingly, sunitinib treatment caused a clear decline in ^{89}Zr-ranibizumab-PET signal in the tumor center, with only minimal reduction of uptake in the tumor rim, with a pronounced rebound after discontinuation. These findings demonstrate that sunitinib treatment effectively inhibits proliferation, neo-vascularization and secondly that ^{89}Zr-ranibizumab-PET is a valuable molecular imaging technique with utility as a biomarker for the determination of intratumoral VEGF status and/or angiogenesis.

Currently MRI and PET imaging are used to visualize antiangiogenic treatment effects mainly by measuring changes in blood flow and permeability (15–17). Preclinically, MRI demonstrated decreased transfer constant K^{trans} following anti-VEGF treatment in a xenografts model, especially in the tumor center (18). High variability in MRI results during follow up of antiangiogenic treatment hampers the predictive value for individual patients (19, 20). PET imaging has a higher sensitivity compared with MRI and allows whole body imaging (21, 22). In this study, we have demonstrated the utility of ^{89}Zr-ranibizumab-PET as a valuable imaging biomarker of the VEGF pathway. Interestingly, if used in patients this PET tracer could also provide insight in changes in VEGF levels in normal organs during sunitinib treatment, which might influence distant invasion after treatment with sunitinib (3).

Rapid blood clearance of ^{89}Zr-ranibizumab and VEGF-driven tissue uptake resulted in high tumor to background ratios that enable more rapid tumor follow up with maximal uptake of ^{89}Zr-ranibizumab in the tumor within 24 hours pi compared with 4 days for ^{89}Zr-bevacizumab. Relatively high kidney uptake of ^{89}Zr-ranibizumab, as seen with other metal labeled proteins, is a consequence of glomerular filtration of the tracer followed by tubular reabsorption and subsequent lysosomal degradation (23, 24). ^{89}Zr-ranibizumab binds with 20–100 fold higher affinity than bevacizumab to all human VEGF-A isoforms, including matrix bound isoforms (6). Most likely, ^{89}Zr-ranibizumab binds like bevacizumab *in vivo* to VEGF located on the cell surface and the extra cellular matrix as shown by Stollman et al. using ^{111}In-bevacizumab in $VEGF_{165}$ and $VEGF_{189}$ over expressing melanoma xenografts (25). Moreover, changes in ^{89}Zr-ranibizumab tumor uptake were 3-fold higher compared with control ^{89}Zr-Fab-IgG, indicating VEGF-mediated tumor uptake. One of our most important findings however, is that ^{89}Zr-ranibizumab tumor uptake can be followed dynamically within the tumor at different time points during and after sunitinib treatment.

^{89}Zr-ranibizumab does not bind to murine VEGF and therefore gives no information about the contribution of mouse VEGF to tumor angiogenesis in our xenografts models. However, our results corresponded highly with the angiogenic state of the tumors shown by other assays, indicating human VEGF to be largely responsible for the angiogenesis effects observed. There was a striking difference between tumor rim and center as uptake demonstrated with VEGF-PET. In concordance with reduced tumor growth, sunitinib treatment resulted in a decrease of angiogenic markers like microvessel density (MVD), as seen in other tumor models (2), vessel diameter, VEGFR2 expression. Further, reduced endothelial proliferation and the absence of pelioses showed true inhibition of angiogenesis. The inhibition of angiogenesis was also associated with high HIF1α and GLUT-1 expression and decreased Ki67 staining, indicating increased hypoxia and cellular stress and reduced tumor cell proliferation. All effects were more pronounced in the center than in the tumor rim, as highlighted by ^{89}Zr-ranibizumab-PET. The ^{89}Zr-ranibizumab-PET signal is the sum of perfusion of the tracer into the tumor followed by binding to VEGF, it is therefore a resultant of changed perfusion, MVD and VEGF expression, reflecting VEGF biodistribution and bioavailability and allowing *in vivo* insight in overall tumor angiogenesis.

VEGF-A staining was performed with an antibody that binds to human all VEGF-A isoforms and to a lesser extent to murine VEGF. The VEGF-A expression, was less intense in the center although we had expected an increase as a result of hypoxia caused by VEGFR inhibition. When we analyzed the plasma level of tumor derived human VEGF in these mice, we observed an initial decrease after 7 days of sunitinib treatment, which matches the results assessed with ^{89}Zr-ranibizumab-PET and underlines the striking finding of initial drop in VEGF expression by tumor cells during sunitinib treatment that has not been reported before. A potential explanation for the initial decrease of VEGF could be an off target effect of sunitinib. Apart from blocking VEGFR signaling, sunitinib binds more than 70 other kinases (26). For instance, it inhibits STAT3, an activator of VEGF transcription, which could explain the initial VEGF reduction (27, 28). Ebos et al. measured already elevated human plasma VEGF levels after 1 week sunitinib treatment in a PC-3 xenograft model (13). We however observed, just after 2 weeks of sunitinib, an enhanced VEGF-PET signal in the tumor rim, which corresponded microscopically with more intense VEGF-A staining, a raise in blood vessel diameter, tumor cell proliferation, and raise in plasma VEGF levels. These results suggest transient antitumor effects as well as dynamic changes in the VEGF pathway resulting in tumor adaptation to sunitinib treatment. These data are in concordance with vessel normalization already 8 days following initiation of the pan-VEGFR-TKI cediranib in a glioblastoma model (19, 29). These results demonstrate the need for noninvasive follow up in continuous as well as intermittent dosing schedules in the clinic to understand the effect of antiangiogenic treatment.

An explanation for the differences observed between the tumor rim and center might be that tumor cells located at the tumor rim are likely not only dependent on tumor blood vessels, but also benefit from adjacent peritumoral blood vessels. Indeed, we did not observe changes in peritumoral blood vessels during sunitinib (Supplement 6), whereas others even observed a large increase in peritumoral blood vessel diameter following cediranib in their glioblastoma model (19). Taken together, our findings emphasize that differences exist in response to antiangiogenic therapy among tumor areas. The interest for biological processes occurring at the edge of the tumor is also attracted by the phenomenon of epithelial mesenchymal transition (EMT) in tumors. EMT contributes to tumor progression and enhances the metastatic potential of tumor cells. It has been proposed that induction of hypoxia is one of the instigators (3, 30, 31). Indeed, sunitinib has showed to increase invasiveness at the tumor boundary and enhanced the forming of metastases (3). VEGF-PET enables noninvasive follow up of this process in the primary tumor as well as in all metastatic lesions.

The strong rebound in ^{89}Zr-ranibizumab-PET signal and rapid tumor regrowth after sunitinib discontinuation reflects what is seen in the clinic. Indeed, comparably to our findings preclinical immunohistochemical analyses have demonstrated rapid revascularization after stopping the VEGFR-TKI AG-013736 (32). Moreover, regrowth of lymph node metastases and flare up of clinical symptoms have been reported during the sunitinib-free period or rapidly after discontinuation (33, 34).

In our study, the clinically most frequently used tracer ^{18}F-FDG did not reflect intratumoral differences or rapid tumor revascularization and regrowth after stopping sunitinib. Furthermore, the homogeneous reduction in ^{18}F-FDG uptake did not correspond with the vitality seen by histology and immunohistochemistry.. In addition, no differences between tumor rim and center were observed in this study with ^{15}O-water after sunitinib despite the clinical feasibility of ^{15}O-water PET to assess baseline tumor perfusion status (35). ^{15}O-water PET performance is partly hampered by a relative low tumor perfusion compared with well perfused organs. For example, in patients 2-fold lower perfusion rates were found in primary renal cell cancers versus normal kidneys (36).

The newly developed VEGF tracer can be clinically used and translate preclinical findings. Recently the first clinical trials have been initiated to visualize VEGF. ^{111}In-bevacizumab visualized all known melanoma lesions in a feasibility study, even very small (1 cm) lesions (37). At this moment serial ^{89}Zr-bevacizumab VEGF-PET scans are performed to study the role of these scans during antiangiogenic treatment in renal cell carcinoma patients (38). When more rapid insight in the dynamic changes in VEGF response in the tumors is required at shorter intervals, ^{89}Zr-ranibizumab offers an additional investigative opportunity.

In conclusion, ^{89}Zr-ranibizumab-PET allows noninvasive dynamic and spatial *in vivo* visualization and quantification of VEGF signaling. ^{89}Zr-ranibizumab-PET therefore has potential use for preclinical and clinical follow up, guidance of new treatment strategies, optimal dose finding, and exploration of drug combinations, to increase the benefit of antiangiogenic therapies.

Disclosure of Potential Conflicts of Interest

The authors declare that no conflict of interest exists.

Acknowledgments

We thank T.H. Oude Munnink, T. Jones, E.M.E. van Straten, and M. Green for technical assistance and helpful comments on the manuscript.

Grant Support

A personal grant to W.B. Nagengast and grants RUG 2007-3739 and RUG 2009-4273 from the Dutch Cancer Society.

Received February 22, 2010; revised August 12, 2010; accepted September 7, 2010; published OnlineFirst November 17, 2010.

References

1. Ferrara N, Gerber HP, LeCouter J. The biology of VEGF and its receptors. Nat Med 2003;9:669–76.
2. Christensen JG. A preclinical review of sunitinib, a multitargeted receptor tyrosine kinase inhibitor with anti-angiogenic and antitumour activities. Ann Oncol 2007;18Suppl 10:x3–10.
3. Paez-Ribes M, Allen E, Hudock J, Takeda T, Okuyama H, Vinals F, et al. Antiangiogenic therapy elicits malignant progression of tumors to increased local invasion and distant metastasis. Cancer Cell 2009;15:220–31.
4. Ebos JM, Lee CR, Cruz-Munoz W, Bjarnason GA, Christensen JG, Kerbel RS, et al. Accelerated metastasis after short-term treatment with a potent inhibitor of tumor angiogenesis. Cancer Cell 2009;15:232–9.
5. Park JE, Keller GA, Ferrara N. The vascular endothelial growth factor (VEGF) isoforms: differential deposition into the subepithelial extracellular matrix and bioactivity of extracellular matrix-bound VEGF. Mol Biol Cell 1993;4:1317–26.
6. Nagengast WB, De Vries EG, Hospers GA, de Mulder, Jr. NH, Hollema H, Brouwers AH, et al. In vivo VEGF imaging with radiolabeled bevacizumab in a human ovarian tumor xenograft. J Nucl Med 2007;48: 1313–9.
7. Hurwitz H, Fehrenbacher L, Novotny W, Cartwright T, Hainsworth J, Heim W, et al. Bevacizumab plus irinotecan, fluorouracil, and leucovorin for metastatic colorectal cancer. N Engl J Med 2004;350:2335–42.
8. Ferrara N, Damico L, Shams N, Lowman H, Kim R. Development of ranibizumab, an anti-vascular endothelial growth factor antigen binding fragment, as therapy for neovascular age-related macular degeneration. Retina 2006;26:859–70.
9. De Vries EG, Meijer C, Timmer-Bosscha H, Berendsen HH, de LL, Scheper RJ, Mulder NH, et al. Resistance mechanisms in three human small cell lung cancer cell lines established from one patient during clinical follow-up. Cancer Res 1989;49:4175–8.
10. Hamacher K, Coenen HH, Stocklin G. Efficient stereospecific synthesis of no-carrier-added 2-[^{18}F]-fluoro-2-deoxy-D-glucose using aminopolyether supported nucleophilic substitution. J Nucl Med 1986; 27:235–8.

11. Verel I, Visser GW, Boerman OC, van Eerd JE, Finn R, Boellaard R, et al. Long-lived positron emitters zirconium-89 and iodine-124 for scouting of therapeutic radioimmunoconjugates with PET. Cancer Biother Radiopharm 2003;18:655–61.
12. Loening AM, Gambhir SS. AMIDE: a free software tool for multimodality medical image analysis. Mol Imaging 2003;2:131–7.
13. Ebos JM, Lee CR, Christensen JG, Mutsaers AJ, Kerbel RS. Multiple circulating proangiogenic factors induced by sunitinib malate are tumor-independent and correlate with antitumor efficacy. Proc Natl Acad Sci U S A 2007;104:17069–74.
14. Keyes KA, Mann L, Teicher B, Alvarez E. Site-dependent angiogenic cytokine production in human tumor xenografts. Cytokine 2003; 21:98–104.
15. Jubb AM, Oates AJ, Holden S, Koeppen H. Predicting benefit from anti-angiogenic agents in malignancy. Nat Rev Cancer 2006;6:626–35.
16. Cai W, Chen X. Multimodality molecular imaging of tumor angiogenesis. J Nucl Med 2008;49Suppl 2:113S–28S.
17. Jain RK. Lessons from multidisciplinary translational trials on anti-angiogenic therapy of cancer. Nat Rev Cancer 2008;8:309–16.
18. O'Connor JP, Carano RA, Clamp AR, Ross J, Ho CC, Jackson A, et al. Quantifying antivascular effects of monoclonal antibodies to vascular endothelial growth factor: insights from imaging. Clin Cancer Res 2009;15:6674–82.
19. Kamoun WS, Ley CD, Farrar CT, Duyverman AM, Lahdenranta J, Lacorre DA, et al. Edema control by cediranib, a vascular endothelial growth factor receptor-targeted kinase inhibitor, prolongs survival despite persistent brain tumor growth in mice. J Clin Oncol 2009; 27:2542—52.
20. Hahn OM, Yang C, Medved M, Karczmar G, Kistner E, Karrison T, et al. Dynamic contrast-enhanced magnetic resonance imaging pharmacodynamic biomarker study of sorafenib in metastatic renal carcinoma. J Clin Oncol 2008;26:4572–8.
21. Perini R, Choe R, Yodh AG, Sehgal C, Divgi CR, Rosen MA, et al. Non-invasive assessment of tumor neovasculature: techniques and clinical applications. Cancer Metastasis Rev 2008;27:615–30.
22. Frangioni JV. New technologies for human cancer imaging. J Clin Oncol 2008;26:4012–21.
23. Behr TM, Goldenberg DM, Becker W. Reducing the renal uptake of radiolabeled antibody fragments and peptides for diagnosis and therapy: present status, future prospects and limitations. Eur J Nucl Med 1998;25:201–12.
24. Backer MV, Levashova Z, Patel V, Jehning BT, Claffey K, Blankenberg FE, et al. Molecular imaging of VEGF receptors in angiogenic vasculature with single-chain VEGF-based probes. Nat Med 2007; 13:504–9.
25. Stollman TH, Scheer MG, Franssen GM, et al. Tumor accumulation of radiolabeled bevacizumab due to targeting of cell- and matrix-associated VEGF-A isoforms. Cancer Biother Radiopharm 2009; 24:195–200.
26. Stein MN, Flaherty KT. CCR drug updates: sorafenib and sunitinib in renal cell carcinoma. Clin Cancer Res 2007;13:3765–70.
27. Xin H, Zhang C, Herrmann A, Du Y, Figlin R, Yu H, et al. Sunitinib inhibition of Stat3 induces renal cell carcinoma tumor cell apoptosis and reduces immunosuppressive cells. Cancer Res 2009;69: 2506–13.
28. Xu Q, Briggs J, Park S, Niu G, Kortylewski M, Zhang S, et al. Targeting Stat3 blocks both HIF-1 and VEGF expression induced by multiple oncogenic growth signaling pathways. Oncogene 2005;24:5552–60.
29. Casanovas O, Hicklin DJ, Bergers G, Hanahan D. Drug resistance by evasion of antiangiogenic targeting of VEGF signaling in late-stage pancreatic islet tumors. Cancer Cell 2005;8:299–309.
30. Pennacchietti S, Michieli P, Galluzzo M, Mazzone M, Giordano S, Comoglio PM, et al. Hypoxia promotes invasive growth by transcriptional activation of the met protooncogene. Cancer Cell 2003;3: 347–61.
31. Polyak K, Weinberg RA. Transitions between epithelial and mesenchymal states: acquisition of malignant and stem cell traits. Nat Rev Cancer 2009;9:265–73.
32. Mancuso MR, Davis R, Norberg SM, O'Brien S, Sennino B, Nakahara T, et al. Rapid vascular regrowth in tumors after reversal of VEGF inhibition. J Clin Invest 2006;116:2610–21.
33. Burstein HJ, Elias AD, Rugo HS, Cobleigh MA, Wolff AC, Eisenberg PD, et al. Phase II study of sunitinib malate, an oral multitargeted tyrosine kinase inhibitor, in patients with metastatic breast cancer previously treated with an anthracycline and a taxane. J Clin Oncol 2008; 26:1810–6.
34. Desar IM, Mulder SF, Stillebroer AB, van Spronsen DJ, van der Graaf WT, Mulders PF, et al. The reverse side of the victory: flare up of symptoms after discontinuation of sunitinib or sorafenib in renal cell cancer patients. A report of three cases. Acta Oncol 20091–4.
35. Saleem A, Price PM. Early tumor drug pharmacokinetics is influenced by tumor perfusion but not plasma drug exposure. Clin Cancer Res 2008;14:8184–90.
36. Anderson H, Yap JT, Wells P, Miller MP, Propper D, Price P, et al. Measurement of renal tumour and normal tissue perfusion using positron emission tomography in a phase II clinical trial of razoxane. Br J Cancer 2003;89:262–7.
37. Nagengast W.B., Lub-De Hooge M.N., Hospers G.A., Brouwers A.H., Hoekstra H.J., Elsinga P.H., et al. Towards clinical VEGF imaging using the anti-VEGF antibody bevacizumab and Fab-fragment ranibizumab. In: Proc Am Soc Clin Oncology Ann. Meeting 2008–3547.
38. Clinical Trial Registration Database. Available from: www.clinicaltrials.gov. Registration number NCT00831857